Results of the Department of Space Physics, Institute of Atmospheric Physics of the Czech Academy of Sciences, published in 2025

1. Polarization Analysis of Type III Langmuir/Z-mode Waves with Coherent Magnetic Component Observations by Solar Orbiter

Observations from the Solar Orbiter spacecraft provide unique insights into the interaction between electron beams and the plasma background in the source regions of type III radio emissions. We analyzed this interaction by examining the high-frequency electric and magnetic components of in situ wave measurements, focusing on their polarization properties. Using electron data from onboard instruments, we modeled the electron velocity distribution function and numerically solved the dispersion relation. We compared the predicted polarization of the electric and magnetic components with the observations. Our findings re consistent with propagation in the Langmuir/Zmode at an oblique wave vector. We explain the magnetic component and transverse polarization by the presence of small density fluctuations, without the need for mode conversion.

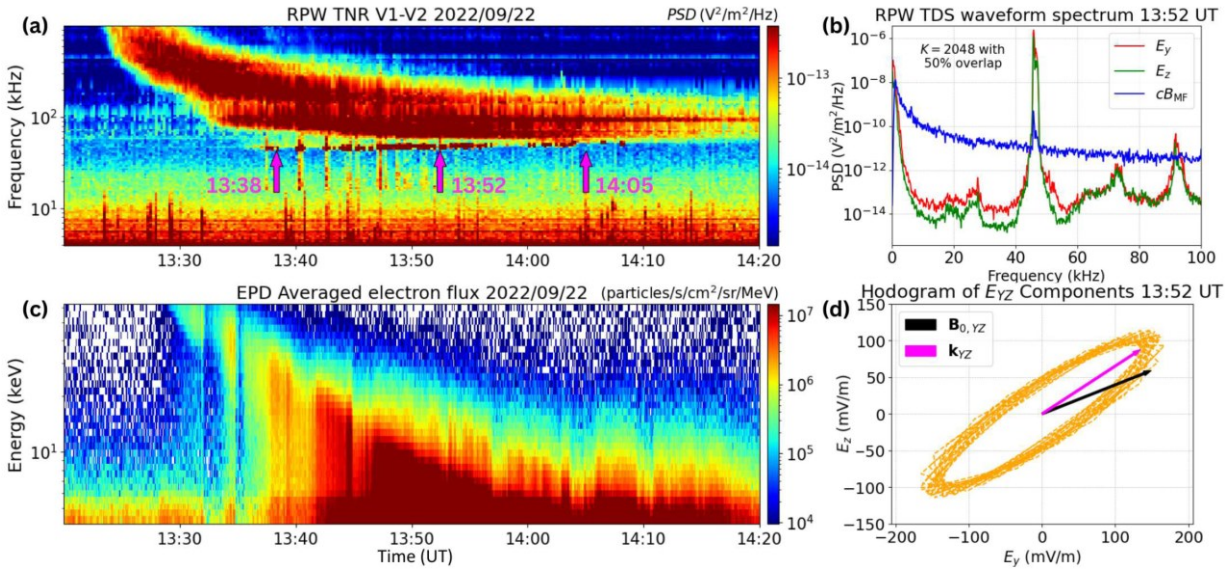

Overview of the type III radio emission on 2022 September 22. (a) The radio emission and Langmuir waves, highlighting three specific timestamps. At 13:38 UT and 14:05 UT, we analyze the electron data, while 13:52 UT marks the strongest Langmuir wave observations. (b) Spectrum of the observed waveform at 13:52 UT, including a coherent high-frequency signal from the search coil magnetometer. (c) The averaged electron Eux from the STEP instrument. (d) A hodogram of the strongest electric field observations (100 samples), with arrows marking the projection of the ambient magnetic field (black) and the predicted wave vector directions.

Reference:

Formánek, T., Santolík, O., Souček, J., Píša, D., Zaslavsky, A., Kretzschmar, M., Maksimovic, M., Owen, C. J., & Nicolaou, G. (2025). Polarization Analysis of Type III Langmuir/Z-mode Waves with Coherent Magnetic Component Observations by Solar Orbiter. *The Astrophysical Journal Letters*, 985(2), L29. https://doi.org/10.3847/2041-8213/add687.

Related references:

Turc, L., Takahashi, K., Kajdic, P., Kilpua, E.K.J., Sarris, T., Palmroth, M., **Souček, J.**, Pfau-Kempf, Y., Dimmock, A., Takahashi, N. (2025). From Foreshock 30-Second Waves to Magnetospheric Pc3 Waves, *Space Science Reviews*, 221, 2, 26. Doi: 10.1007/s11214-025-01152-y.

Krupař, V., Kontar, E.P., **Souček, J.**, Wilson, L. B., Szabo, A., Krupařová, O., Reid, H.A.S., **Hajoš, M., Píša, D., Santolík, O.**, Maksimovic, M., & Pickett, J. S. (2025). First Detection of Low-frequency Striae in Interplanetary Type III Radio Bursts. The Astrophysical Journal Letters, 985(2), L27. https://doi.org/10.3847/2041-8213/add688

2. A Dataset of Lower Band Whistler Mode Chorus and Exohiss with Instrumental Noise Thresholds

In this work, we presented a large database of natural electromagnetic emissions of lower band whistler mode chorus and exohiss within the Earth's magnetosphere. It is based on more than 124 million selected survey measurements of magnetic fluctuations, recorded between 2001 and 2020 by the two NASA Van Allen Probes and four ESA Cluster spacecraft. The database provides a comprehensive view of amplitudes of these important electromagnetic emissions in the audible frequency range. We carefully conditioned the data to minimize the influence of instrumental artefacts. We also removed all data points which might have be contaminated by instrumental noise using a newly developed method to define detection thresholds as a function of frequency, time, and instrument settings. The database can serve as a valuable resource for a broad range of scientists studying space weather, magnetospheric physics, and radiation belt dynamics.

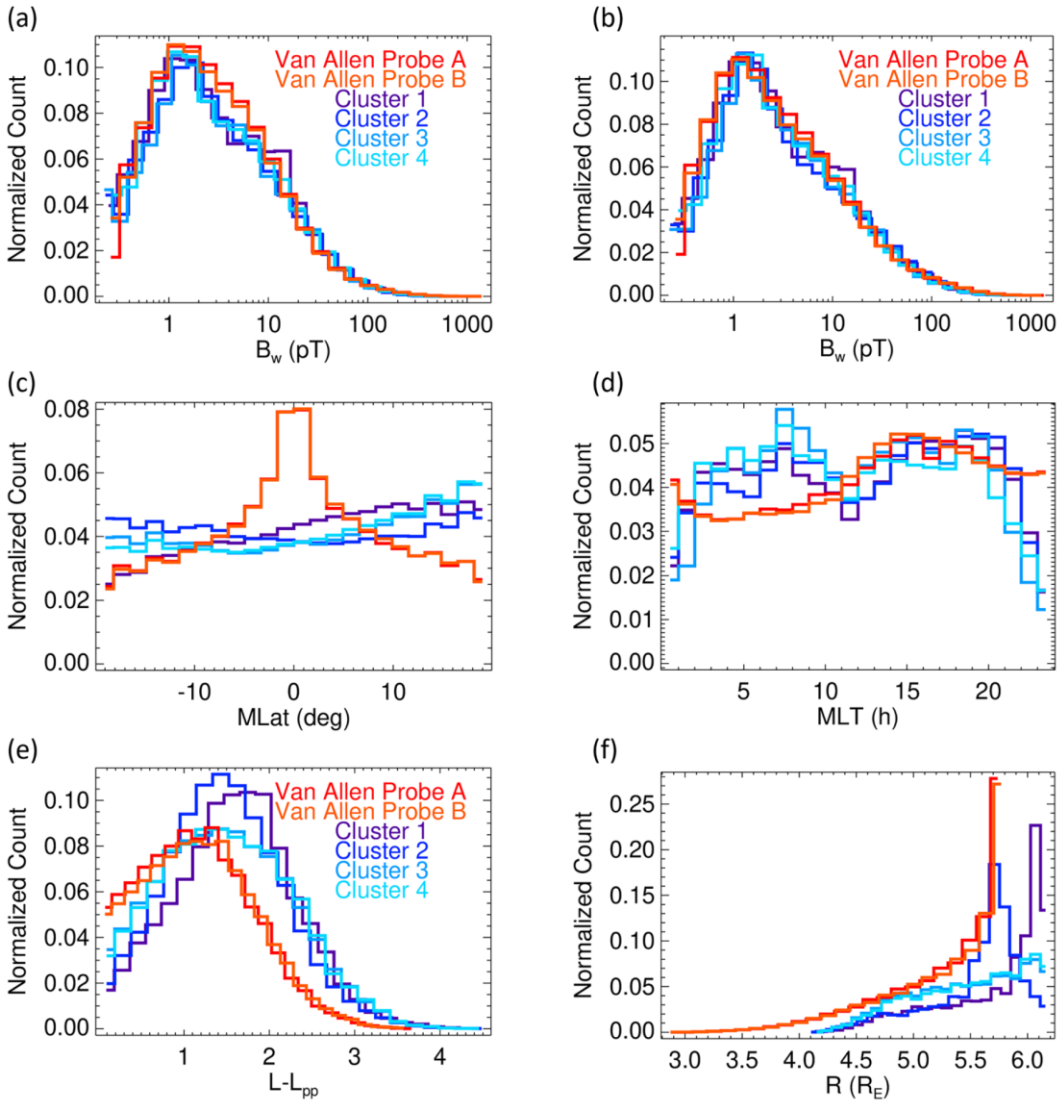

Distributions root-mean-square amplitudes and spatial coverage of overlapping measurements of lower-band chorus and exohiss. Color coded distributions are given for datasets from Table 3 from the paper. (a) Distributions of root-mean-square amplitudes Bw, (b) the same but for the restricted datasets on the morning side with magnetic local time of 0–12 h, (c) distributions of magnetic latitudes for the datasets from panel a, (d) distributions of magnetic local time, (e) distributions of equatorial distances from the model plasmapause, (f) distributions of radial distances, all for the datasets from panel a. Histograms in 25 logaritmic bins are always normalized by the total number of measurements.

Reference:

Santolík, O., Kolmašová, I., Taubenschuss, U., Hanzelka, M., & Hartley, D.P. (2025). A Dataset of Lower Band Whistler Mode Chorus and Exohiss with Instrumental Noise Thresholds.
Sci Data, 12 (1), 1265. Doi:10.1038/s41597-025-05531-6.

Related references:

Němec, F., **Santolik**, O., Albert, J. M. (2025). VLF Transmitter Signals Observed by the Cluster Spacecraft Over a Wide Range of Latitudes, *J. Geophys. Res. Space Physics*, 130, e2024JA033621. Doi:10.1029/2024JA033621.

Tachi, K., Katoh, Y., **Santolík, O.** (2025). Whistler-Mode Chorus Wave Duct Propagation Caused by Ultralow Frequency Wave: Event Analysis and Ray-Tracing Simulation. *Geophys. Res. Lett.*, 52 (17), e2025GL116840. Doi:10.1029/2025GL116840.

Martinez-Calderon, C., Shiokawa, K., **Santolík, O.**, Kurita, S., Keika, K., Connors, M., Schofield, I., **Hanzelka, M.**, Kurth, W.S. (2025). Simultaneous ground-satellite observations of ELF/VLF emissions generated by a strong magnetospheric compression. *Earth Planets Space*, 77 (1), 49. Doi:10.1186/s40623-025-02170-4.

Hartley, D.P., Chen, L., Gu, W., Christopher, I.W., & **Santolik, O.** (2025). The Impact of Plasma Density Gradients on Lower Band Chorus Wave Propagation. *Geophys. Res. Lett.*, 52 (6), e2024GL113258. Doi:10.1029/2024GL113258.

Ampuku, Y., Tsuchiya, F., Kurita, S., Kasaba, Y., Katoh, Y., Fukizawa, M., Miyoshi, Y., Shinohara, I., Kasahara, Y., Matsuda, S., Kumamoto, A., Matsuoka, A., Kitahara, M., & **Santolík, O.** (2025). Ducted Propagation of Whistler Mode Waves Observed by the Arase Satellite. *J. Geophys. Res. Space Phys*., 130 (5), e2024JA033359. Doi:10.1029/2024JA033359.

Remya, B., Halford, A. J., Noh, S. J., Fernandes, P. A., **Grison, B.**, Wang, D., et al. (2025). (Un)Explained EMIC waves: Understanding quiet time EMIC wave drivers. *J. Geophys. Res. Space Phys*, 130, e2024JA033125. Doi:10.1029/2024JA033125.

Timmermann, G., Fischer, D., Auster, H.-U., Richter, I., **Grison, B.**, and Plaschke, F. (2025). Comparison of noise levels of two magnetometer types and their suitability for different space environments, *Geosci. Instrum. Method. Data Syst*., 14, 447–458. Doi:10.5194/gi-14-447-2025.

3. Localization of the Cluster satellites in the geospace environment

The geometry of the terrestrial magnetized environment, or geospace, varies widely in space and time due to the Earth's magnetic field interactions with the interplanetary medium. A spacecraft's location in geospace is only approximately determined by its coordinates since the environment is inhomogeneous, with distinct physical processes occurring in different regions. Knowing the location in the geospace offers a strong support for data analysis. This paper introduced a new dataset, Geospace Region and Magnetospheric Boundary identification (GRMB), which provides labelled positions for each Cluster spacecraft over the whole mission, with respect to the local environment. This continuous labelling is based on manual selection, supported by browsing 44 different Cluster data products. The GRMB dataset

includes 15 labels spanning from the plasmasphere to solar wind regions. Its consistency was validated over 7 years against reference lists and by the physical properties of the GRMB regions. Over those years, Cluster spent a similar proportion of the time (≈15%) in the regions labelled lobe, plasmasheet, plasmasheet transition region, magnetosheath and solar wind.

Location of the Cluster-1 spacecraft in year 2007 (orbits 1001 to 1154) according to the GRMB dataset.

Reference:

Grison, B., Darrouzet, F., Maggiolo, R., **Hajoš, M., Dvořák, M., Švanda, M., Jeřábková, A**., Graham, M., Taylor, G.T., Herment, D., Masson, A., **Souček, J., Santolík, O.**, & De Keyser, J. (2025). Localization of the Cluster satellites in the geospace environment. *Scientific Data* 12, 327. Doi:10.1038/s41597-025-04639-z.

4. Nonlinear acceleration of ultrarelativistic electrons in the outer radiation belt disrupted by transverse wave modulations

Whistler-mode waves scatter ultrarelativistic electrons in the radiation belts and accelerate them through resonant interactions. In simplified models, nonlinear phase trapping by high-amplitude waves can increase electron energy by several MeV within seconds. However, the acceleration rate in realistic wave packets is slower due to small-scale wave field structures reducing trapping efficiency. While previous studies focused on short field-aligned amplitude modulations and phase jumps, we examine the effects of transverse modulations, which have been observed to reach scales comparable to ultrarelativistic electron gyroradii. Using test-particle simulations, we demonstrated that these modulations disrupt the acceleration process. Our numerical results suggest that nonlinear trapping plays a negligible role in

accelerating electrons above a certain energy limit, reinforcing the diffusive nature of wave-driven electron transport at multi-MeV energies. Unlike field- aligned structures, transverse phase incoherence modifies the effective wave spectrum and allows for resonance, making amplitude modulations a necessary component for suppression of acceleration.

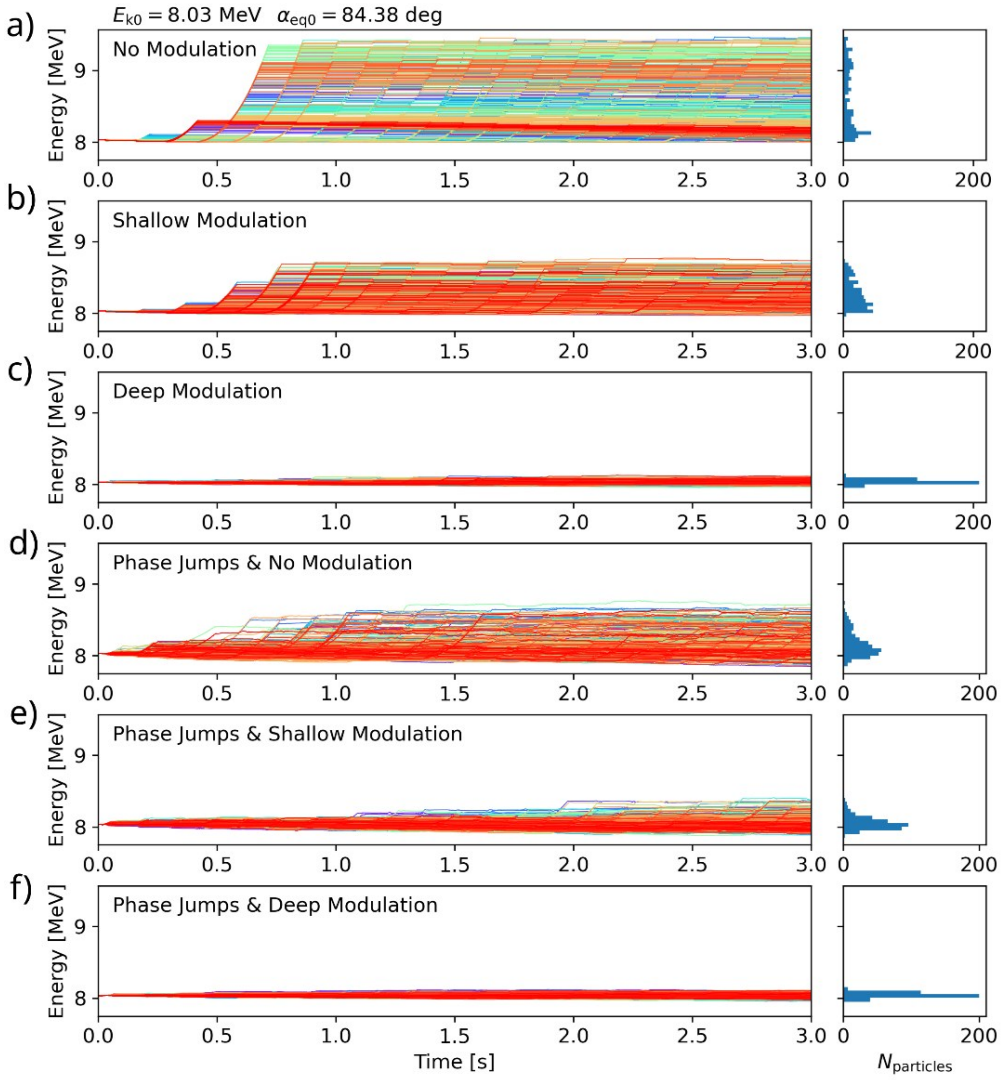

Evolution of electron energy for initial energy and pitch angle of 8.03 MeV and 84.38°. The first column shows individual electron trajectories color-coded by initial gyrophase, while the second column presents energy histograms at t = 3 s. (a–c). Various modulation depths without phase jumps at amplitude minima. (d–f) Wave models with phase jumps.

Reference:

Hanzelka, M., Shprits, Y. Y., & **Santolík, O.** (2025). Nonlinear acceleration of ultrarelativistic electrons in the outer radiation belt disrupted by transverse wave modulations. *Geophysical Research Letters*, 52, e2025GL116883. Doi:10.1029/2025GL116883.

Related references:

Ma, Q., Li, W., Bortnik, J., **Hanzelka, M.**, Gan, L., Artemyev, A. V., & Shen, X.-C. (2025). Diffusive and nonlinear scattering of ring current protons by electromagnetic ion cyclotron waves in the Earth's inner magnetosphere. *J. Geophys. Res. Space Physics*, 130, e2025JA034078. Doi:10.1029/2025JA034078.

Shen, X., Li, W., Ma, Q., Qin, M., Capannolo, L., **Hanzelka, M.**, Angelopoulos, V., Artemyev, A., Wilkins, C, Liu, J., & Tsai, E. (2025). Whistler mode wave-driven electron scattering properties from ELFIN measurements of the precipitation ratio. *J. Geophys. Res. Space Physics*, 130(4), e2024JA033363. Doi: 10.1029/e2024JA033363.

5. Effects of fine spectral structure of chorus emissions on nonlinear scattering and acceleration of radiation belt electrons

Whistler-mode chorus waves play a crucial role in accelerating electrons in Earth's outer radiation belt to relativistic and ultrarelativistic energies. While this electron evolution is typically modeled using a diffusion approximation for scattering, high-amplitude chorus waves induce nonlinear resonant effects that challenge this approach on short time scales. The long-term influence of these nonlinear interactions on radiation belt dynamics remains an unresolved issue. Recent simplified models suggest rapid nonlinear acceleration to ultrarelativistic energies, with formation of butterfly distributions during parallel wave propagation. In this study, we introduced a novel numerical approach based on Liouville phase space density mapping to investigate nonlinear scattering by high-amplitude waves over extended periods (minutes and beyond). We use a numerical wave field model of lower-band chorus risers that includes realistic fine-spectral features including subpacket modulations, phase decoherence, and jumps in wave normal angle. By incorporating these detailed spectral characteristics of the waves, we demonstrate that the rapid acceleration occurs across a broader pitch-angle range, forming a flat-top distribution. Similar effect is observed as the repetition period of chorus elements becomes shorter, with the additional effect of increased electron precipitation due to transition from bursty to continuous flux profiles in the loss cone. These findings highlight the importance of incorporating nonlinear effects and fine-scale wave properties in the future development of high-energy electron models for the outer radiation belt.

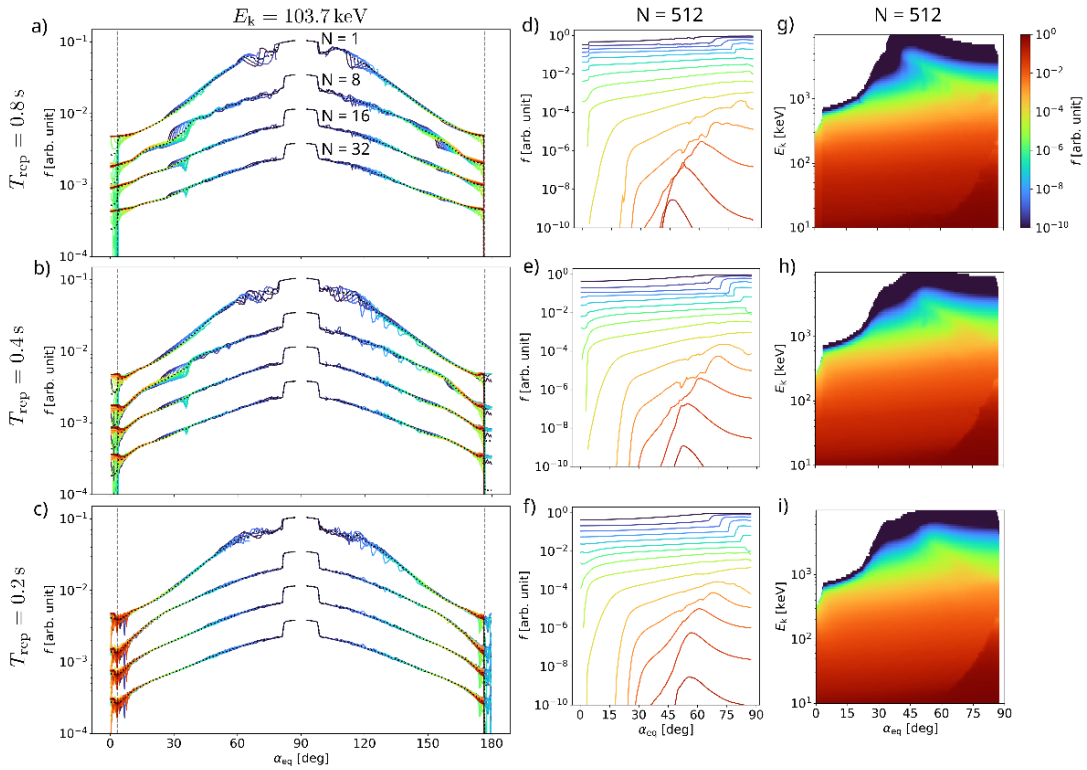

The effects of chorus repetition period Trep on the phase space density (PSD) evolution, with each row corresponding to one of the three values 0.8 s, 0.4 s, and 0.2 s. In all three cases, the wave field is parametrized by 2σω = 0 Ωe0, 2σϑ = 0°. The first column (panels a–c) shows the state of local PADs at four different time points given by the number of cycles N = {1, 8, 16, 32}; the energy value is always the same, Ek = 104.7 keV. As the number of cycles increases, the PSD values are multiplied by 1/3 each time to fit all lines into one plot without major overlaps. The second column (panels d–f) shows the PADs at N = 512 across several energy levels coded by color, with the same legend as in Figure 5. The dashed gray lines in panels a–f represent the equatorial loss cone. The third column (panels g–i) shows the two-dimensional PSD distribution in energies and equatorial pitch angles as a heat map.

Reference:

Hanzelka, M., Shprits, Y., Wang, D., Haas, B., **Santolík, O.**, & Gan, L. (2025). Effects of fine spectral structure of chorus emissions on nonlinear scattering and acceleration of radiation belt electrons *J. Geophys. Res. Space Physics*, 130(4), e2024JA033382. Doi: 10.1029/e2024JA033382

Related references:

Qin, M., Li, W., Nishimura, Y., Huang, S.,Ma, Q., **Hanzelka, M.**, Capannolo, L., Shen, X., Angelopoulos, V., An, X., Artemyev, A., & Gan (2025). Sub-MeV Electron Precipitation Driven by EMIC Waves in Plasmaspheric Plumes at High L Shells L. *J. Geophys. Res. Space Physics*, 130(3), e2025JA033756. Doi: 10.1029/e2025JA033756.

Gan, L., Li, W., Albert, J., **Hanzelka, M.**, Ma, Q., & Artemyev, A. (2025). Inhomogeneity Ratio for Nearly Field-Aligned Electrons Interacting With Whistler-Mode Waves *J. Geophys. Res. Space Physics*, 129(10), e2024JA032554. Doi: 10.1029/2024JA032554.

6. Rapid evolution of energetic lightning strokes in Mediterranean winter storms

The occurrence of winter lightning concentrates in a few specific regions in the world, including the Mediterranean, where electromagnetic signatures of this interesting dangerous phenomenon have not yet been studied in detail. We investigate the initial stage of energetic negative cloud-to-ground winter lightning flashes in the West Mediterranean region using broadband magnetic field measurements (5 kHz–90 MHz) recorded in winter 2014/2015, which was unusually rich in global lightning activity. We found that the winter pre-stroke processes leading to the high peak current lightning (<−100 kA) lasted on average only 1.7 ms (in one case only 220 μs). Rapid evolution of energetic lightning indicates that leader initiation charge centers can be as low as 500m above the ground. The measured distribution of pre-stroke pulse amplitudes and interpulse intervals can be used to model the charge structure in the lower thundercloud dipole and to derive the properties of in-cloud lightning channels.

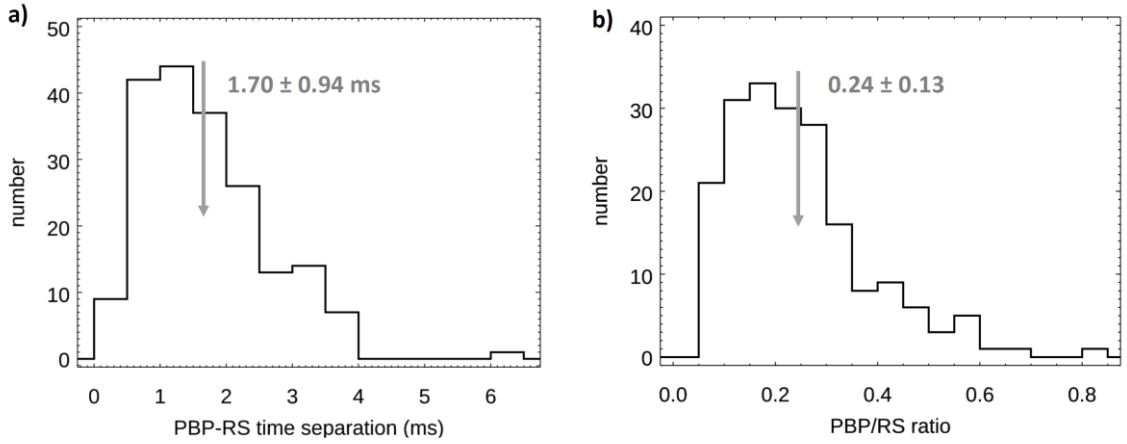

a) Distribution of time separations of the first pre-stroke pulse and the return stroke pulse. b) Distribution of ratio of the amplitudes of the largest pre-stroke pulse and the returns stroke pulse.

Reference:

Kolmašová, I., Santolík, O., Kolínská, A. et al. (2025). Rapid evolution of energetic lightning strokes in Mediterranean winter storms. *npj Climate and Atmospheric Science* 8, 71. Doi:10.1038/s41612-025-00965-6.

Related references:

Linzmayer, V., F. Němec, **Santolík, O., Kolmasova, I.** (2025). Lightning-Induced Electron Precipitation Events Observed at Low Altitudes, *J. Geophys. Res. Space Physics*, 130, e2024JA033639. Doi: 10.1029/2024JA033639.

7. Post-Return Stroke VHF Electromagnetic Activity in North-Western Mediterranean Cloud-to-Ground Lightning Flashes

We investigated properties of the electromagnetic activity following the first lightning return stroke (RS), using concurrent observations from the SLAVIA (Shielded Loop Antenna with a Versatile Integrated Amplifier) sensor, the lightning mapping array (LMA) SAETTA (Suivi de l'Activité Electrique Tridimensionnelle Totale de l'Atmosphère) and Météorage LF network in the Corsica region. From the data collected between September and December 2015, we selected 66 negative cloud-to-ground (-CG) and 26 positive cloud-to-ground (+CG) lightning flashes in the north-western Mediterranean region. In the SAETTA data, we observed a decrease of the Very High Frequency (VHF) radiation rate and the VHF power as recorded within a typical 80-µs time window at the LMA stations, immediately after the RS pulse in 59 -CG flashes. Contrastingly, we showed that all examined +CG flashes exhibit a rapid increase of the VHF radiation rate and the VHF power immediately after the RS. We suggested a possible explanation of this phenomenon by considering step-like propagation of a negative part of bidirectional leader starting at the top end of the positive lightning channel inside the thundercloud, emitting electromagnetic radiation across a broad frequency spectrum.

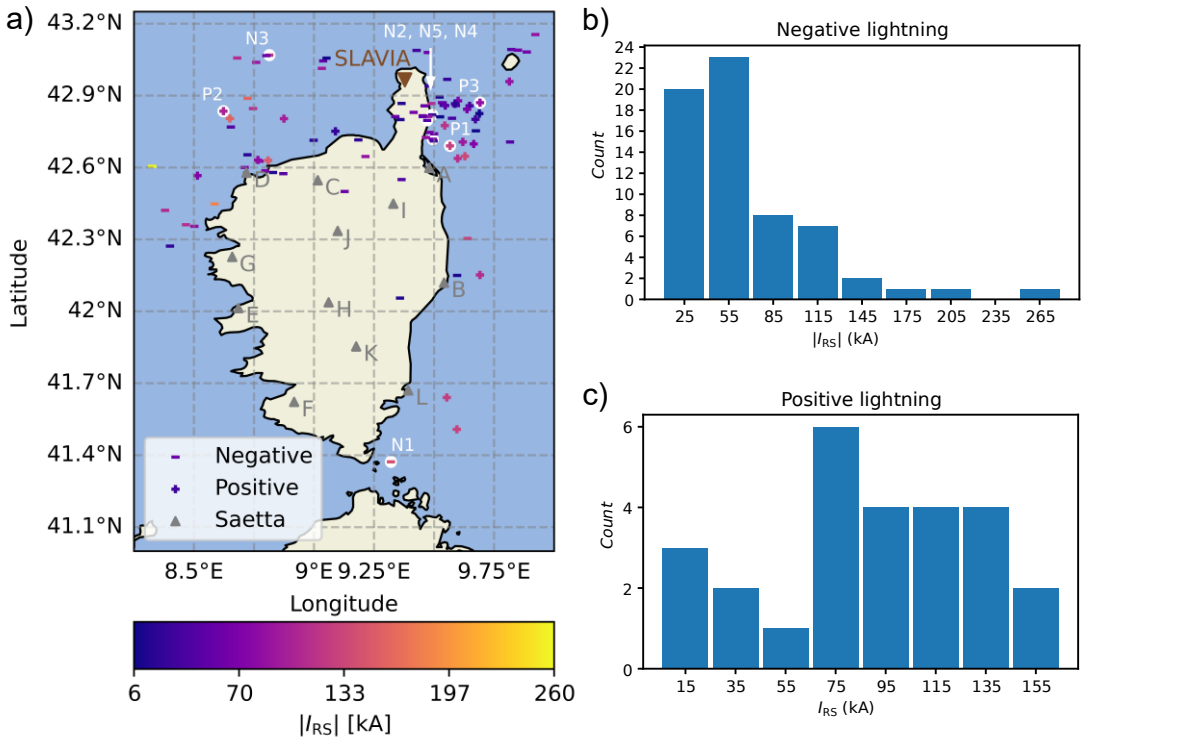

a) Map of all 1st return strokes used in this study as located by Météorage. The color corresponds to the absolute value of the first RS peak current IRS for each flash. The SAETTA stations are labelled by grey triangles with their corresponding letter name, while the SLAVIA sensor is marked as a brown reversed triangle. Cartographic outline denotes the island of Corsica and the northern part of Sardinia. b) Histogram of the absolute value of first RS peak current |IRS| for all 66 -CG flashes; c) histogram of IRS for all 26 +CG flashes.

Reference:

Kolínská, A., Kolmašová, I., Defer, E., **Santolík, O., & Pédeboy, S**. (2025). Post-return stroke VHF electromagnetic activity in north-western Mediterranean cloud-to-ground lightning flashes, *Atmospheric Chemistry and Physic*s, 25, 1791–1803. Doi:10.5194/acp-25-1791-2025.

8. A Global Map of Average Electron Densities in the Magnetosphere of Saturn

Measurements from the Cassini Radio and Plasma Wave Science (RPWS) experiment obtained during the entire orbital phase of the Cassini mission around Saturn (13.2 years) are processed into a meridional map of plasma densities, comprising the innermost region of the ring ionosphere, the Enceladus plasma torus, and the outer magnetosphere, up to a dipole L-shell of 30. We combined data from RPWS wave observations, such as whistler-mode waves and upper hybrid electrostatic emissions, and from the RPWS Langmuir probe when operated in the proxy mode, providing an estimate for the spacecraft potential. In the region between dipole L-shells of 2.4 and 30, observed electron densities are described by an analytic model that fits two functions, one for the water group ions and one for the protons, to observed densities across latitude on each magnetic field line. The derived electron density profiles are then augmented by a model for the cold core electron temperature as a function of L-shell to obtain a meridional map of the electrostatic potential of the ambipolar electric field. The potential is extrapolated to the inner region of the rings, i.e., to below L = 2.4, to solve for the distribution of electron density in the ring ionosphere. A solution is based on a diffusive equilibrium model for the electrons and two ion species, and on observations from Cassini along the Saturn Orbit Insertion trajectory. A combination of analytic and diffusive equilibrium results finally yields an average global picture for the distribution of electron density in Saturn's magnetosphere.

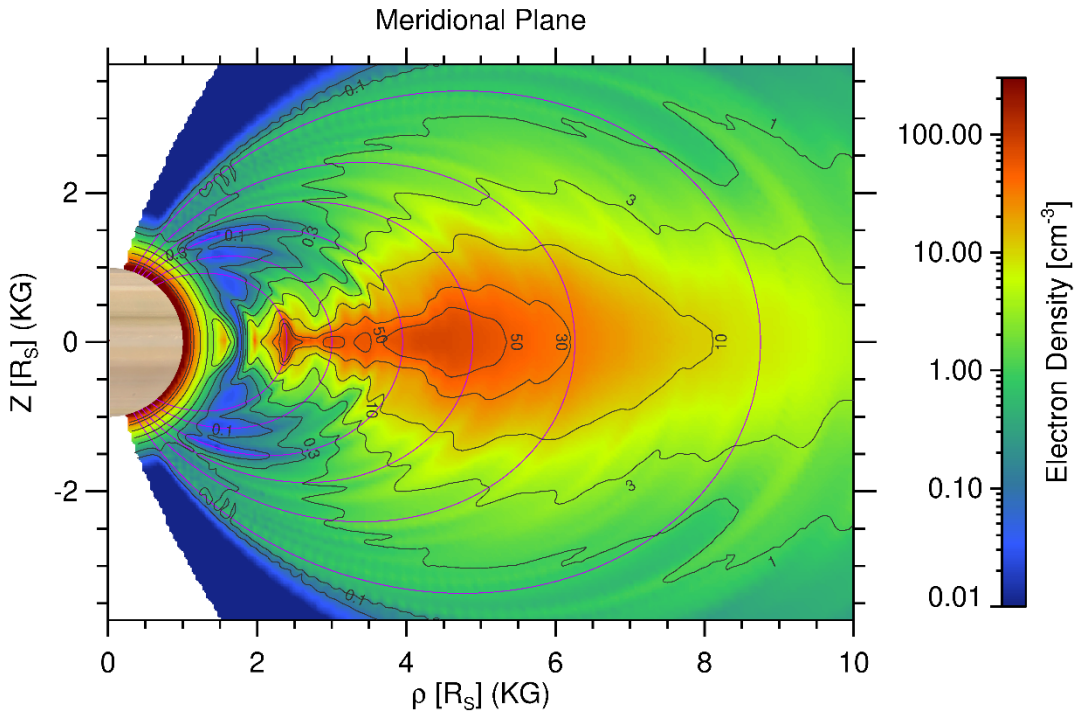

Meridional distribution of electron density in the inner magnetosphere of Saturn from the model of Taubenschuss et al. (2025). Prominent features are the Enceladus plasma torus, stretching between equatorial distances ρ of 3 - 10, density peaks connected to the rings (inside ρ = 3 Rs), a plasma void above the B ring, and a high-latitude plasmapause. Planetary magnetic dipole field lines are overplotted in purple color.

Reference:

Taubenschuss, U., O. Santolík, D. Píša, M. Imai, G. Fischer, S. Wu, M. W. Morooka, and W. S. Kurth (2025), A Global Map of Average Electron Densities in the Magnetosphere of Saturn, *J. Geophys. Res. Space Physics*, 130, e2025JA034007. Doi:10.1029/2025JA034007.

Related references:

Kurth, W. S., A. H. Sulaiman, J. E. P. Connerney, F. Allegrini, P. Valek, R. W. Ebert, C. Paranicas, G. B. Clark, N. Kruegler, G. B. Hospodarsky, C. W. Piker, S. Kotsiaros, **M. Imai**, and S. J. Bolton (2025). Juno Observations of Io's Alfvén Wing from 23 Io Radii, *Geophys. Res. Lett*., 52, e2025GL115497, doi:10.1029/2025GL115497.

Fischer, G., **M. Imai, U. Taubenschuss, D. Píša**, and W. S. Kurth (2025). The radio wave polarization of Saturn lightning observed by Cassini, *J. Geophys. Res. Space Physics*, 130, e2024JA033560, doi:10.1029/2024JA033560.

Fischer, G., U. **Taubenschuss, D. Píša, M. Imai**, and W. S. Kurth (2025). Spectral structures of Jovian broadband kilometric radiation revealed by Cassini and Juno, *J. Geophys. Res. Space Physics*, 130, e2024JA032826, doi:10.1029/2024JA032826.

Rabia, J., Hadid, L. Z., André, N., Nénon, Q., Chust, T., **Píša, D.**, Parsec-Wallis, A., Coates, A. J., & Rymer, A. M. (2025). Cassini CAPS-ELS Observations of Low-Energy Electron Beams Within Enceladus Mid-Latitude Flux Tubes. *Geophys. Res. Lett*., 52(22), e2025GL119448. Doi:10.1029/2025GL119448.

9. Description of instrumentation for missions with IAP involvement

We contributed to the different instrumental papers related to active mission to Jupiter and its icy moons (JUICE), to terrestrial magnetospheric cusps mission (TRACERS) and to the large X /ray ESA mission ATHENA.

References:

Wahlund, J.-E., Bergman, J. E. S., Åhlen, L., (...), **Santolík, O., Souček, J.**, Štverák, Š., **Grison, B., Jánský, J., Kolmašová, I., Lán, R., Píša, D., Taubenschuss, U., Uhlíř,** L. et al. (2025). The Radio & Plasma Wave Investigation (RPWI) for the JUpiter ICy moons Explorer (JUICE), *Space Sci. Rev.*, 221, 1, 1. Doi:0.1007/s11214-024-01110-0.

Masters, A., Modolo, R., Roussos, E., Krupp, N., Witasse,(….) **Santolík, O**. et al. (2025). Magnetosphere and Plasma Science with the Jupiter Icy Moons Explorer. *Space Sci. Rev.*, 221 (2), 24. Doi:10.1007/s11214-025-01148-8.

Trattner, K.J., LaBelle, J., **Santolík, O.**, Kletzing, C.A., Miles, D.M., Fuselier, S.A., Bonnell, J.W., Bounds, SR., **Kolmašová, I.**, Petrinec, S.M., Sawyer, R.P., Vines, S.K., Moser-Gauthier, C., Cairns, IH., & Yeoman, T.K. (2025). From the TRICE-2 Investigations to the TRACERS Mission. *Space Sci. Rev.*, 221, 52. Doi:10.1007/s11214-025-01178-2.

Miles, D.M., Kletzing, C.A., Fuselier, S.A., Goodrich, K.A., Bonnell, J.W., Bounds, (…), Hospodarsky, G.B., Jaynes, A.N., Labelle, J., Lin, Y., Øieroset, M., Petrinec, S.M., Phillips, M.L., Powers, B., Prasad, R., Rospos, A., **Santolík, O**., et al. (2025). The Tandem Reconnection and Cusp Electrodynamics Reconnaissance Satellites (TRACERS) Mission. *Space Sci. Rev.*, 221 (5), 61. Doi:10.1007/s11214-025-01184-4.

Petrinec, S.M., Kletzing, CA., Miles, D.M., Fuselier, S.A., Christopher, I.W., Crawford, D., Omar, S., Bounds, S.R., Bonnell, J.W., Halekas, J.S., Hospodarsky, G.B., Strangeway, R.J., Lin, Y., Trattner, K.J., Labelle, J.W., Øieroset, M., **Santolík, O.**, Moen, J., Oksavik, K., Yeoman, T.K., Cairns, I.H., & Mark, D. (2025). The Tandem Reconnection and Cusp Electrodynamics Reconnaissance Satellites (TRACERS) Mission Design, *Space Sci. Rev.*, 221 (5), 60. Doi:10.1007/s11214-025-01185-3.

Hospodarsky, G.B., Carton, A.J., Dvorsky, R.T., Kirchner, D.L., Miles, D.M., Bounds, S.R., Christopher, I.W., Crawford, D., Deasy, K., Dolan, J.S., Faden, J.B., Fessenden, G.W., Hansen, C., Helland, R.L., Klinkhammer, S.D., Miller, M.C., Morris, K.J., Piker, C.W., **Santolík, O.,** Steele, K., Tompkins, T.A., Webb, M.D., & Wilkinson, D. (2025). The Magnetic Search Coil (MSC) on the TRACERS Mission, *Space Sci. Rev.*, 221 (5), 72. Doi:10.1007/s11214-025-01200-7.

Peille, P., Barret, D., Cucchetti, E., Svoboda, J., Brigitte, M., **Souček, J., Lán, R., Taubenschuss, U., Uhlíř, L**. et al. (2025). The X-ray integral field unit at the end of the Athena reformulation phase, *Experimental Astronomy*, 59, 2, 18. Doi: 10.1007/s10686-025-09984-w.

Department of Space Physics, Institute of Atmospheric Physics of the Czech Academy of Sciences in 2025

1. Radka Balková, secretary, 50% FTE
2. Kateřina Barotová, student, 50% FTE since 1 February 2025
3. Praveen Basuvaraj, 70% FTE PhD student since 1 April 2025, 100% FTE postdoctoral associate since 1 July 2025
4. Adam Boudouma, postdoctoral associate, since 10 February 2025
5. Tomáš Formánek, student, from 1 July 2025 till 27 August 2025, otherwise on leave in Observatoire de Paris
6. Benjamin Grison, research scientist
7. Michajlo Hajoš, research scientist
8. Miroslav Hanzelka, postdoctoral associate since 15 October, otherwise on leave at GFZ Potsdam
9. Pavel Houfek, research engineer, PhD student
10. Samia Ijaz, postdoctoral associate, since 8 October 2025
11. Masafumi Imai, research scientist
12. Jiří Jánský, research engineer
13. *Michaela Jírová, PhD student, on parental leave*
14. Petr Kašpar, research scientist
15. Vavřinec Kavan, student, 20% FTE
16. Andrea Kolínská, PhD student, since 1 October 2025 postdoctoral associate
17. Ivana Kolmašová, senior research scientist
18. *Vratislav Krupař, research scientist, on leave in NASA GSFC*
19. *Oksana Krupařová, research scientist, on leave in NASA GSFC*
20. Radek Lán, research engineer
21. Ján Mičko, PhD student, 70% FTE
22. David Píša, research scientist
23. Martin Popek, TLE observer, 25% FTE
24. Kateřina Rosická, PhD student, 80% FTE
25. Ondřej Santolík, senior research scientist, head of the department
26. Jan Souček, senior research scientist, deputy head of the department
27. Kohki Tachi, PhD student, visiting from 1 October 2025, 70% FTE since 10 December 2025
28. Ulrich Taubenschuss, research scientist
29. Luděk Uhlíř, research engineer
30. Jaroslav Vojta, research engineer, 10% FTE